



1 **Ion acceleration at dipolarization fronts associated with**
2 **interchange instability in the magnetotail**

3 **Chao Sun¹, Yasong Ge², Haoyu Lu^{1,3}**

4 *¹School of Space and Environment, Beihang University, Beijing,*
5 *100191, China (lvhy@buaa.edu.cn)*

6 *²Institute of Geology and Geophysics, Chinese Academy of Sciences,*
7 *Beijing, 100029, China*

8 *³Lunar and Planetary Science Laboratory, Macau University of*
9 *Science and Technology – Partner Laboratory of Key Laboratory of*
10 *Lunar and Deep Space Exploration, Chinese Academy of Sciences,*
11 *Macau, 519020, China*

12
13
14 **Abstract** It has been confirmed that dipolarization fronts (DFs) can be a
15 result from the existence of interchange instability in the magnetotail. In
16 this paper, we used a Hall MHD model to simulate the evolution of the
17 interchange instability, which produces DFs on the leading edge. A test
18 particle simulation was performed to study the physical phenomenon of
19 ion acceleration on DF. Numerical simulation indicates that almost all
20 particles move towards the earthward and dawnward and then drift to the
21 tail. The DF-reflected ion population on the duskside appears earlier as a
22 consequence of the asymmetric Hall electric field. Ions, with dawn-dusk



23 asymmetric semicircle behind the DF, may tend to be accelerated to a
24 higher energy ($>13.5\text{keV}$). These high-energy particles are eventually
25 concentrated in the dawnside. Ions experience effective acceleration by the
26 dawnward electric field E_y while they drift through the dawn flank of the
27 front towards the tail.

28



29 **Introduction**

30 Earthward moving high-speed plasma flows, which are called bursty bulk
31 flows (BBFs), play a vital important role in carrying significant amounts
32 of mass, energy, and magnetic flux from the reconnection region to the
33 near-Earth magnetotail (Angelopoulos et al., 1994). BBFs are often
34 accompanied with a strong (~ 10 nT), abrupt (several seconds), transient
35 enhancement of the magnetic field component B_z in the leading part,
36 known as a dipolarization front (DF) (Nakamura et al., 2009; Sergeev et
37 al., 2009; Fu et al., 2012a). Ahead of the DF, a minor B_z dip usually be
38 observed by THEMIS and MMS (Runov et al., 2009; Schmid et al., 2016),
39 which may be typically interpreted as strong diamagnetic currents caused
40 by a plasma pressure drop over the front or magnetic flux passing over
41 the SC or transient reconnection (Kiehas et al., 2009; Ge et al., 2011;
42 Schmid et al., 2011). Simulations have suggested that the magnetic
43 energy would be transferred to plasma on the DF layer in the B_z dip
44 region ahead of trailing fronts (Lu et al., 2017). Many of studies show
45 that the passage of a magnetic island (Ohtani et al., 2004), jet braking
46 (Birn et al., 2011), transient reconnection (Sitnov et al., 2009; Fu et al.,
47 2013), and/or the interchange/ballooning instability (Guzdar et al., 2010;
48 Pritchett and Coroniti, 2013) may account for DF generation. Both
49 Cluster and MMS observed that DFs propagate not only earthward but
50 also tailward, since the fast-moving DFs are compressed and reflected,



51 three quarters of the DFs propagate earthward and about one quarter
52 tailward (Zhou et al., 2011; Nakamura et al., 2013; Huang et al., 2015;
53 Schmid et al., 2016).

54 Spacecraft observations showed that the sudden energy increase in
55 charged particle fluxes at DFs from tens to hundreds of keV in the
56 magnetotail (Runov et al., 2011; Zhou et al., 2010; Fu et al., 2011; Li et
57 al., 2011; Artemyev et al., 2012). A series of studies have been conducted
58 to understand the signatures of DFs and particles, as well as the particle
59 acceleration mechanisms on the DFs. Li et al., (2011) studied the force
60 balance between the Maxwell tension and the total pressure gradient
61 surrounding the DF and found that the imbalance between the curvature
62 force density and the pressure gradient force density would lead to the
63 flux tube acceleration. Ions, essentially nonadiabatic in the magnetotail,
64 can be directly accelerated along the electric field produced by earthward
65 convection of the front, such as due to surfing acceleration or shock drift
66 acceleration (Birn et al., 2012, 2013; Ukhorskiy et al., 2013; Artemyev et
67 al., 2014). Electrons, comparatively adiabatic over most of their orbits,
68 can be accelerated through betatron and Fermi process (Birn et al., 2004,
69 2012). It is noticed that the magnetic field amplitude behind DF is much
70 greater than that ahead of it, Zhou et al. (2011, 2014) obtained that the
71 earthward moving front can reflect and accelerate ions. Ukhorskiy et al.
72 (2013, 2017) took the magnetic field component B_z for different areas



73 and situations into account, revealing a new robust acceleration
74 mechanism enabled by stable trapping of ions. In most cases, ions are
75 energized by combined actions from different acceleration mechanisms.
76 Nevertheless, the physical processes that generate suprathermal particles
77 are not yet fully understood.

78 On the simulation ground, previous two-dimensional simulations just
79 unveil large scale physical process concerning DFs, in their models, the
80 electric field (most of them are derived from $-V \times B$) is assumed to be
81 solely in the y direction behind DFs (Ukhorskiy et al., 2012; Greco et al.,
82 2014; Zhou et al., 2014). It has been found that the spatial scale of DFs in
83 the dawn-dusk direction is about 1-3 R_E and its thickness is on the order
84 of the ion inertial length (Runov et al., 2011; Schmid et al., 2011), which
85 would be between 500 and 1000 km. In the sub-proton scale, there is an
86 electric field directed normal to the DF. The frozen-in condition is broken
87 at the DF and the electric field is mainly attributed by the Hall and
88 electron pressure gradient terms, with the Hall term dominants (Fu et al.,
89 2012b; Lu et al., 2013; Lu et al., 2015). Therefore, the Hall MHD model
90 is necessary to obtain the Hall electric field, which may determine the
91 electric system on DFs.

92 Lu et al. (2013) have successfully simulated the DF associated with
93 interchange instability in the magnetotail and the trend of simulated
94 physical variables are in good agreement with observations. In this paper,



95 we improves the simulation model in order to study how the Hall electric
96 field on DFs acts on the particle trajectories and ion energizations. Since
97 the DF is produced by temporal evolution of interchange instability
98 self-consistently, it would be meaningful to understand the ion
99 acceleration mechanism associated with the interchange instability in the
100 magnetotail.

101

102 **Theoretical and Numerical Model**

103 Numerical simulations have proved that the existence of interchange
104 instability triggered by the tailward gradient of thermal pressure and the
105 earthward magnetic curvature force is a possible generation mechanism
106 of the DFs in the magnetotail (Guzdar et al., 2010). Based on the Hall
107 MHD model associated with interchange instability (Lu et al., 2013), we
108 conducted test particle simulations to track ions trajectories backward in
109 time.

110 Our simulation was performed by two steps, the first is to establish a
111 more realistic DF to get particle motion background. The other is to place
112 test particles and track their trajectories.

113 The simulation coordinate system is defined with the x-axis pointing
114 away from the Earth, the y-axis pointing from dusk to dawn, and the
115 z-axis pointing northward (Guzdar et al., 2010, Figure 1). The breaking of
116 the earthward flow together with the curvature of the vertical field leads



117 to an effective gravity g away from the earth. Dimensional units are based
 118 on a magnetic field of 15 nT, the Alfvén velocity of 750 km/s, and
 119 reference length of $1 R_E$ leading to a time unit of ~ 8.5 s, an electric field
 120 of 11.25 mV/m, and a pressure unit of 0.179 nPa.
 121 The dimensionless model with an effective gravity is as follows:

$$\begin{aligned}
 & \frac{\partial}{\partial t} \begin{bmatrix} \rho \\ \rho \mathbf{U} \\ \mathbf{B} \\ \rho e_t \end{bmatrix} + \nabla \cdot \begin{bmatrix} \rho \mathbf{U} \\ \rho \mathbf{U} \mathbf{U} + P \mathbf{I} - \frac{\mathbf{B} \mathbf{B}}{\mu_m} \\ \mathbf{U} \mathbf{B} - \mathbf{B} \mathbf{U} \\ (\rho e_t + P) \mathbf{U} - \frac{\mathbf{B}}{\mu_m} (\mathbf{U} \cdot \mathbf{B}) \end{bmatrix} = \begin{bmatrix} 0 \\ g \\ 0 \\ g U \end{bmatrix} + \\
 & d_i \begin{bmatrix} 0 \\ 0 \\ -\frac{1}{\mu_0} \nabla \times \left(\frac{\nabla \times \mathbf{B} \times \mathbf{B}}{\rho} \right) \\ -\frac{1}{\mu_0^2} \mathbf{B} \cdot \left[\nabla \times \left(\frac{\nabla \times \mathbf{B} \times \mathbf{B}}{\rho} \right) \right] \end{bmatrix} + d_i \begin{bmatrix} 0 \\ 0 \\ -\frac{1}{\mu_0} \nabla \times \left(\frac{\nabla \rho_e}{\rho} \right) \\ -\frac{1}{\mu_0^2} \mathbf{B} \cdot \left[\nabla \times \left(\frac{\nabla \rho_e}{\rho} \right) \right] \end{bmatrix} \quad (1)
 \end{aligned}$$

123 Where $P = p + \mathbf{B}^2/2\mu_0$, \mathbf{U} and \mathbf{B} are velocity vector and magnetic
 124 field vector, respectively, $\rho e_t = \rho \mathbf{U}^2/2 + p/(\gamma - 1) + \mathbf{B}^2/2\mu_0$, β is
 125 plasma beta, g_x is the effective gravitational force in x direction. In
 126 equation (1), the second and third terms on the right-hand side represent
 127 the Hall effect and the electron pressure gradient, respectively. In our
 128 present numerical cases, we postulate that plasma is under isothermal
 129 conditions with an isothermal equation of state $p = \beta \rho/2$ and take the
 130 adiabatic exponent $\gamma = 5/3$. The ion inertial length $d_i =$
 131 $(m_i/\mu_0 e^2 Z^2 L^2 n_i)^{1/2}$, given the reference length $L = 1 R_E$, the
 132 dimensionless ion inertial length is taken as $d_i \approx 0.1$. Electron pressure



133 p_e is taken as $p/6$, because the proton temperature is 5 times that of
 134 electron temperature (Baumjohann et al., 1989; Artemyev et al., 2011).
 135 As for initial conditions, the quasi-stationary equilibrium built by the
 136 plasma pressure and effective gravity g (see equation (2)) (Guzdar et al.
 137 2010 and Lu et al. 2013, 2015) is theoretically reasonable.

$$138 \quad \hat{g} \frac{\beta}{2} = \frac{\partial}{\partial x} \left(\frac{\beta}{2} \rho + \frac{B_z^2}{2} \right) \quad (2)$$

139 It should be noticed that the dawn-dusk and earthward electric field
 140 components averagely, increase to ~ 5 mV/m along with the transient B_z
 141 increase and in some events, the electric field increase exceeded 10
 142 mV/m (Runov et al., 2009, 2011; Schmid, D., et al. 2016). However, the
 143 electric fields calculated by the Hall MHD model in Lu et al. (2013) are
 144 smaller than the observations (see Lu et al., 2013, for a typical
 145 dipolarization event at $x = -10 R_E$ in the equatorial plane, we set $B_0 = 15$
 146 nT, leading to B_z changed from 10.2 nT to 16.8 nT after DF propagation.
 147 The electric field components E_x and E_y are both less than 3 mV/m). So,
 148 it is reasonable that we improve the initial conditions to obtain a realistic
 149 electric field, which plays a vital important role in ion energization.

150 We take the initial conditions as follows:

$$151 \quad \rho(x) = \frac{1}{2}(\rho_L + \rho_R) - \frac{1}{2}(\rho_L - \rho_R) \tanh\left(\frac{x}{l}\right) \quad (3)$$

$$152 \quad \begin{cases} B_z(x) = 0.28x + 0.7535 & (x \leq -0.38) \\ B_z(x) = 1.5 + \tanh\left(\frac{x}{0.3}\right) & (-0.38 < x < 0.4) \\ B_z(x) = 0.14x + 2.314 & (x \geq 0.4) \end{cases} \quad (4)$$

153 Given the generalized Ohm's law, we use a piecewise function to



154 describe B_z so as to obtain a strong electric field. In equation (3), ρ_L
155 and ρ_R are the density closer to and away from the Earth, respectively
156 and the characteristic scale $l = 0.2 R_E$.
157 We solved equation (1) by adopting the second-order upwind total
158 variation diminishing scheme. The simulation box is $2 R_E$ and $1.5 R_E$ in
159 the direction of x and y , respectively. The x boundary is assumed to be
160 zero for all perturbed quantities and the y boundary is to be periodic.
161 As the second simulation step, the control equations for ion motion
162 should be given. Typically, the drift approximation breaks down in terms
163 of ion motion in magnetotail. The dimensionless equations of motion are
164 given by

$$165 \quad \begin{cases} \frac{d\mathbf{r}}{dt} = \mathbf{u} \\ \frac{d\mathbf{u}}{dt} = \alpha(\mathbf{E} + \mathbf{V} \times \mathbf{B}) \end{cases} \quad (5)$$

166 where \mathbf{r} is the particle position, \mathbf{u} is the particle velocity, the
167 dimensional parameter $\alpha = \frac{1}{d_i} \approx 10$.

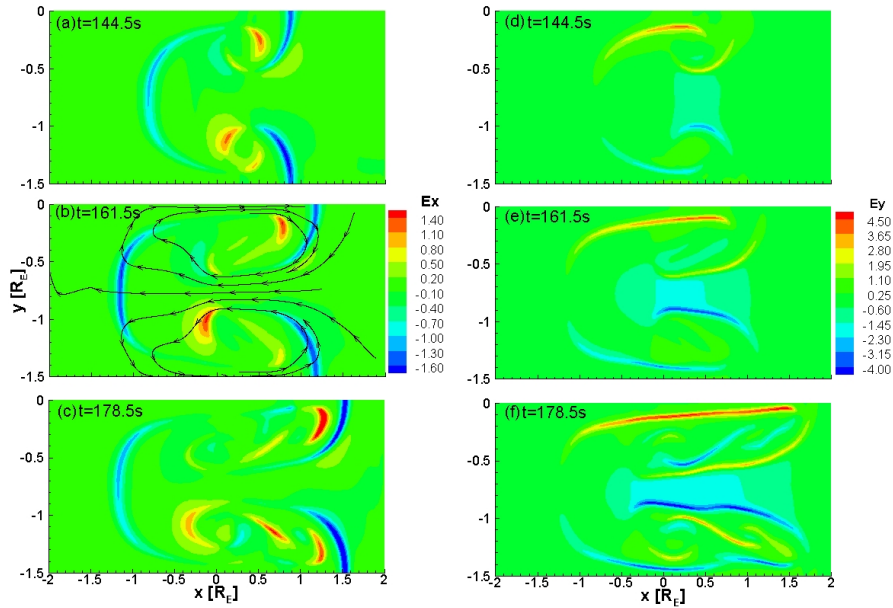
168

169 **Simulation Results**

170 From 0s to 144.5s, the simulation experienced a pre-onset phase, during
171 which the DF formed as a consequence of effective gravity g interaction
172 with plasma density gradient. In order to be more realistic, we set up the
173 time interval from 144.5s to 187s as the acceleration period of the
174 particles.



175 Figure 1 shows the evolution of the electric field in the $z = 0$ plane and
176 black lines indicate streamlines, one can clearly see that the DF moves
177 toward the Earth as time passes by. From Figure 1b it can be seen that the
178 earthward flows coexisted with the tailward flows of the dawn and dusk
179 edges, as a consequence two vortex flow pattern appeared. Figure 1 also
180 shows that the electric field components E_x and E_y are both normal to the
181 front, which is consistent with the observation and simulation (Fu et al.,
182 2012b; Lu et al., 2013). It should be noticed that the electric field is
183 asymmetrically distributed on the DF, with a stronger dawnside electric
184 field. This asymmetry can be interpreted that the two vortexes produce
185 the convection electric field in the direction of dusk-dawn, which
186 generate superposition and cancellation of the dawn and dusk side electric
187 field of DF respectively.



188
 189 **Figure 1.** Evolution of the electric field E_x (a-c) and E_y (d-f), black line
 190 in (b) indicate streamlines
 191 At $t = 144.5s$, we numerically distribute test particles (80000 ions in total)
 192 around the DF (a simulation box with $x = -0.9 R_E \sim -0.4 R_E$, $y = -1.46 R_E$
 193 $\sim -0.04 R_E$) with the initial power law energy distribution $F \sim (1 +$
 194 $h/\kappa T_0)^{-\kappa-1}$ (we take $\kappa = 5$, $T_0 = 1.5 keV$ and h from 1 keV to 10 keV)
 195 (Artemyev et al., 2015). Figure 2 exhibits the spatial distribution of
 196 protons at a given moment. The energy of particles is marked with color
 197 and black lines indicate the position of DFs. As time passes by, the ions
 198 behind the DF accelerate and transport to the dawn flank of the DF,
 199 resulting in the reduction of the ion density behind the DF. We investigated
 200 the characteristics of ions trajectories and found that the behaviors of ions
 201 consist of two parts (not shown), one is forced by the electric field E_x at



the leading edge of the front, resulting in earthward motion and
 dawnward drift. Another is due to the electric field E_y at the dawn flank
 of the DF, leading to tailward drift. These results are consistent with
 observations and simulations (Nakamura et al., 2002; Greco et al., 2014;
 Zhou et al., 2011, 2014). Therefore, the electric field on the DF (Figure
 1a), mainly produced by Hall term and always normal to the front (Fu et
 al., 2012b; Lu et al., 2013), makes the particles move in the way
 described above. Statistical analysis of the ions energy in Figure 2
 indicates that the maximum energy is about 27 keV. In order to better
 distinguish particles from different energy, we assumed that the ions with
 the final energy greater than 13.5 keV are high-energy particles.

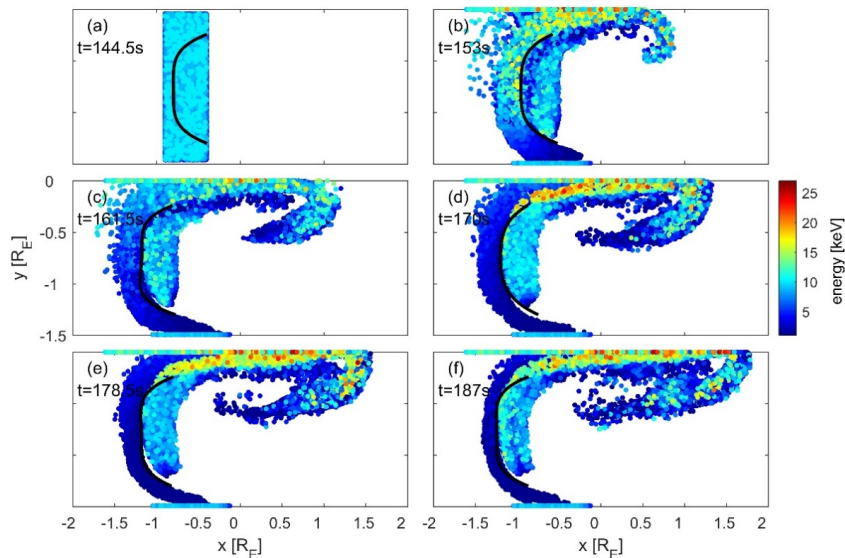
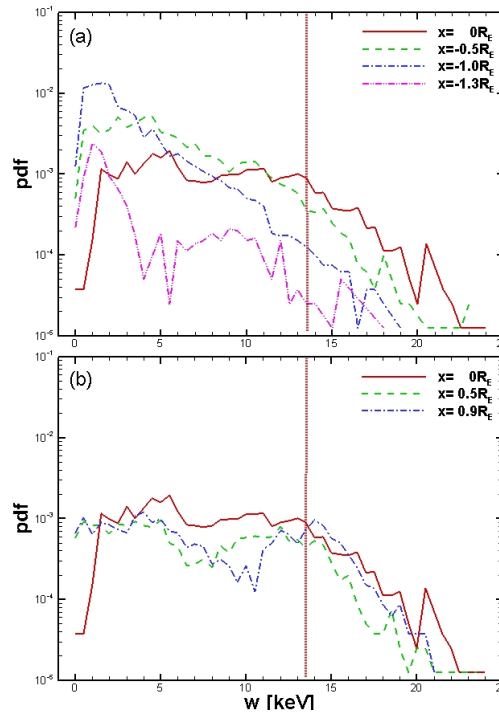


Figure 2. Test particle simulations of proton energization at the DF,
 particle energy is indicated with color and black line represents the
 position of the DF



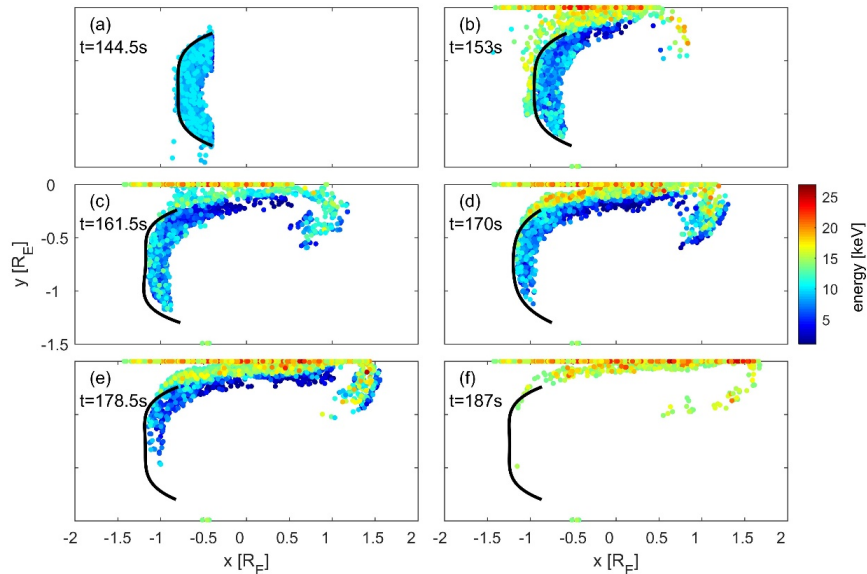
217

218 **Figure 3.** PDFs of particle energy computed at the region of (a) $x < 0 R_E$
 219 and (b) $x > 0 R_E$. The red dotted line mark the high energy demarcation
 220 line 13.5 keV.

221 Figure 3 gives the probability density function (PDF) of particle energy at
 222 different x positions. In order to better distinguish the curves of different
 223 x distances among the multiple fold lines, we show the results in two
 224 figures according to different region in x direction. It can be seen from
 225 Figure 3b that the high-energy particles are assembled in the region of $x >$
 226 $-0.5 R_E$ whereas Figure 3a shows that the small energy (~ 2 keV) ions are
 227 concentrated in the region of $x < -0.5 R_E$. At $x = 0 R_E$, ion energy is
 228 evenly distributed between 2 keV and 16 keV practically. In combination



229 with Figure 2, we can further obtain that almost all the high-energy
 230 particles gathered in the dawnside of $x > -0.5 R_E$ region. It implies that
 231 ion acceleration is more effective at the dawnside of DF.
 232 To have a statistical description of high-energy ions, we picked out
 233 high-energy particles from the total number. The simulation results are
 234 shown in Figure 4 with ions energy marked with different color. It
 235 appears that high energy particles, accounting for 6 percent, mainly
 236 gathering at the dawnside of the DF.



237
 238 **Figure 4.** Snapshots of high-energy ions at specific moment of the
 239 simulation, black line represents the position of the DF
 240 Figure 4a shows that the initial position of high-energy particles is
 241 roughly an asymmetric semicircle whereas the dawnside area is wider
 242 than the duskside, which means that more ions are accelerated in the



243 dawnside than in the duskside. Compared with Figure 2, however, we can
244 intuitively infer that ions with initial positions ahead of or behind and
245 away from the front would not obtain great energization. The ions with
246 initial positions ahead of the front are forced by the E_x of pre-DF region
247 and they move earthward and dawnward with a larger gyration radius due
248 to smaller ambient magnetic B_z , thus can't be accelerated by the
249 dawnside electric field E_y . The ions with initial positions behind the front
250 move with it and always stay behind the DF during the whole evolution
251 period of DF. As a result, there exist no strong fields to energized ions.
252 That is to say, only particles which diverted to the dawnside region closer
253 to the front can be effectively accelerated.

254 In a previous paper, Zhou et al. (2014) inferred that the more energized
255 DF-reflected ions originating from the duskside of the DF would be able
256 to reach farther into the ambient. In their model the ions would have been
257 accelerated more significantly in the DF duskside than in its dawnside
258 which is due to the y displacements behind the convex DF (Zhou et al.,
259 2014 Figure 3). However, observations and numerical simulations
260 indicate that the convective electric field behind the front is smaller than
261 the Hall term on the DF on the spatial scale of ion inertial length (Fu et al.,
262 2012b). Therefore, the explanation based on the convective electric field
263 E_y was inappropriate in our model. Figure 4 has already illustrated that
264 the ion acceleration process is on the dawnside. In addition, statistical



analysis of 4863 high-energy ions indicates that 1570 ions were traced to the duskside of the DF, about 32 % of the total high-energy particles. The source area of ions reaches closer to the Earth, as shown in Figure5.

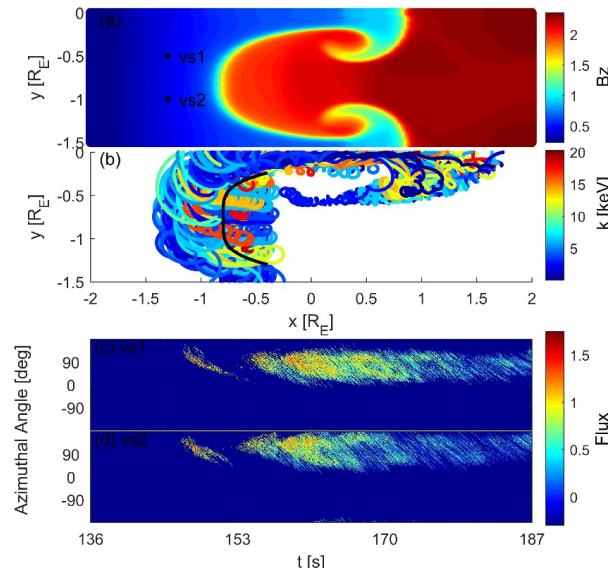


Figure 5. Simulation results of ion differential energy fluxes in the 1-20 keV energy range at different location. (a) Positions of virtual satellites. (b) Ions with initial positions on different y distances moving with the dipolarization front, the DF at $t = 144.5$ s was marked with black solid line. Kinetic energy at final moment is marked with color. (c and d) Energy fluxes at dawnside (vs1) and duskside (vs2), respectively, as the functions of equatorial azimuthal angle and time. The dark spots in Figure 5a mark the locations of the virtual satellites. Figure 5c and 5d show the distribution of differential energy flux as the function of equatorial azimuthal angle and time at the duskside and dawnside of the DF respectively. Ion trajectories with initial positions



280 along different y distances in Figure 5c and 5d are plotted in Figure 5b
281 where the DF at $t = 144.5$ s is set as baseline and marked with black solid
282 line. Kinetic energy at final moment is indicated with color.

283 It is obviously seen in Figure 5 that the duskside ions tend to move to
284 dawn at the front (Figure 5d, $90^\circ < \theta < 180^\circ$), while the dawnside ones
285 divert toward tailward (Figure 5c, $0^\circ < \theta < 90^\circ$). This finding is similar
286 to the fluxes of 78-300 keV protons in Birn et al. (2015). At about $t =$
287 146s ~153s, the particles with higher initial energy ahead of the front
288 have large radius of gyration and those particles are minor affected by the
289 smaller initial electric field, therefore they are almost simultaneously
290 observed (Figure 5b and 5d). While at $t > 153$ s ions with the initial
291 position at duskside would be able to reach farther into the ambient,
292 which is consistent with the results of Zhou et al. (2014) and Birn et al.
293 (2015). On the other hand, the earlier observed ions are not the most
294 energized ions compared with high-energy counterparts in our model,
295 which is opposite to Zhou's conclusion. It can be easily understood by
296 considering the Hall electric field. The small electric field near the
297 duskside of the front allows particles to drift toward earthward and
298 dawnward for a long time, whereas the high one close to dawnside forces
299 ions to drift tailward quickly during the period that particles obtain most
300 energy (Figure 4).

301 In order to study how the Hall field E_y on the dawnside of DF accelerate



ions, we choose one typical ion to track its trajectory, which is initiated at $x = -0.7 R_E$, $y = -0.86 R_E$ behind the DF with an azimuth angle of 14.58° and initial kinetic energy of 1 keV. Its final kinetic energy is 12 keV, as shown in Figure 6. Figure 7 demonstrates the evolution of ion positions and energy. During the beginning period from 144.5s to 162s, the ion moves earthward together with the front and meanwhile downward in the frame of the moving front. During this period, the ion gains very little energy. Even though the E_x component of electric field accelerates the ion along its earthward motion, the deceleration by the E_y component keeps the ion energy almost unchanged. When $t = 163.2$ s, the ion arrives at the dawnside of the DF, where the Hall electric field is very strong. After a sharp energization for about 3 seconds, the ion kinetic energy increase to ~ 10 keV (Figure 7b and 7c, the weaker E_x works to reduce the energy by about 8 keV and the stronger E_y increases the energy by about 20 keV). As shown in Figure 6 and 7 that after $t > 166$ s the ion kinetic energy gradually increases, which can be interpreted that the y-displacement δy^+ (corresponding to the energy increase) is larger than δy^- (corresponding to the energy reduction) in the case where E_y component is almost constant.

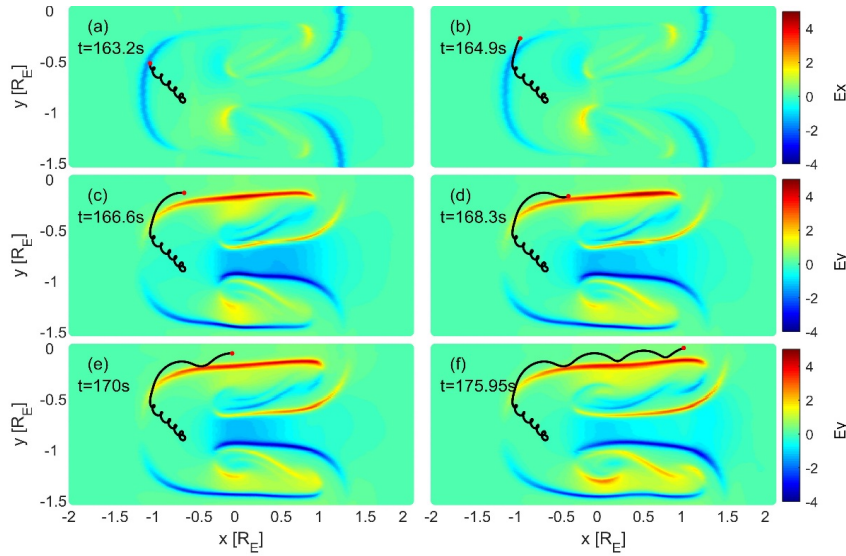


Figure 6. Orbits of a proton with the initial energy 1 keV and final energy 12 keV, traced from $x = -0.7 R_E$, $y = -0.86 R_E$ at different moments. The locations of proton are shown as red dots superposed on snapshots of the background Hall electric field E_x (a-b) and E_y (c-f).

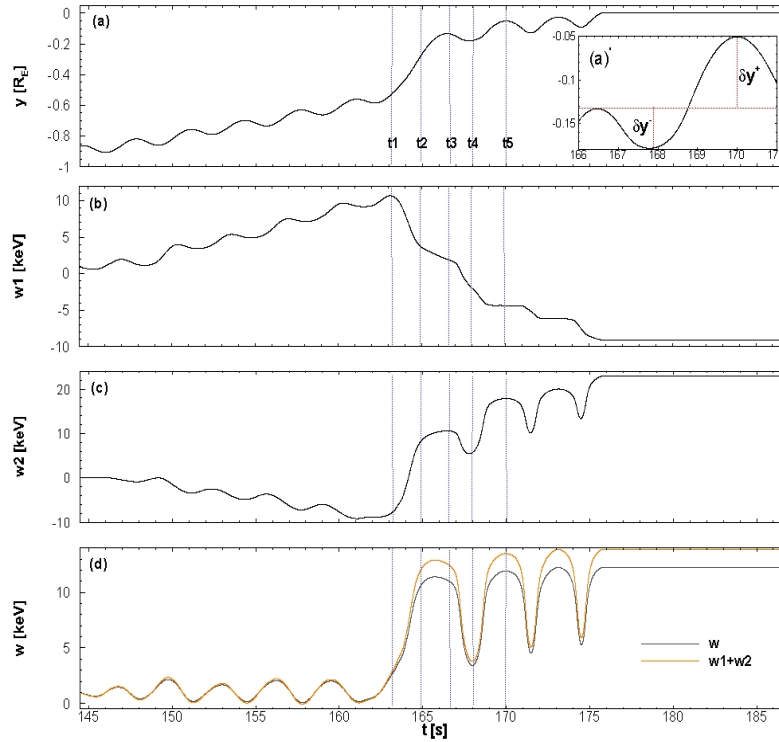


Figure 7. Physical quantities of ion as the function of time with blue dotted lines index specific moment. (a), (a') Y position and its partial enlarged detail, red dotted line is the reference line. (b, c) Energization produced by E_x and E_y , respectively. (d) Kinetic energy and numerical summation of w_1 and w_2 display with orange and black line, respectively. The label of t_1 to t_5 correspond to 163.2s, 164.9s, 166.6s, 168s and 170s respectively.

Summary and Discussion

In this paper, we used a test particle simulation to investigate ion acceleration at dipolarization fronts (DFs) produced by interchange



337 instability in the magnetotail, by performing a Hall MHD simulation. The
338 Hall MHD model was improved by applying the realistic initial
339 conditions to obtain the fields which are better consistent with
340 observation.

341 Test particles were settled in both the pre-DF and post-DF region, most of
342 them exhibited earthward and dawnward drift and then diverted tailward.
343 It is found that ions with the initial position at duskside would be able to
344 reach farther into the ambient plasma, which has been also proofed by
345 Zhou et al. (2014) and Birn et al. (2015). Statistical analysis shows that
346 the high-energy particles are mainly assembled in the dawnside of $x >$
347 $-0.5 R_E$ region, which suggests the dawnside region of the DF is the main
348 area for particle acceleration.

349 Numerical simulation results indicate that the ions initially settled behind
350 the front may obtain higher energization. In order to explain how the Hall
351 electric field influence ions, we tracked the trajectory of particular ions in
352 the ion-scale electric field. As expected, the E_y component at the dawn
353 flank of DF plays an important role in the acceleration of ion. Although
354 the E_x component in the pre-DF region constitutes a potential drop of ~ 1
355 keV across the DF as reported by Fu et al., (2012b), the energy
356 enhancement would be offset on their way out toward the magnetotail due
357 to the E_y component. The spatial and temporal properties of E_y
358 component are critical factors for particle acceleration (Greco et al., 2014;



359 Birn et al., 2013, 2015; Artemyev et al., 2015; Ukhorskiy et al., 2017). In
360 contrast to the results from other MHD model, it makes sense in our
361 self-consistent Hall MHD simulation that the accelerating electric field is
362 the E_y component of the Hall electric field on the dawnside of the front
363 instead of the convection electric field E_y behind the front in their model.
364 Our two-dimensional Hall MHD model can well reproduce the direct
365 acceleration process generated by the Hall field. Nevertheless, it should
366 be pointed out that the ion acceleration mechanisms such as Fermi
367 acceleration and resonance acceleration can also provide powerful ion
368 energization with tens of keV to hundreds of keV (Fu et al., 2011;
369 Artemyev et al., 2012), which is not discussed in this paper. Still, there is
370 no doubt that our study suggests that the dawn flank dusk-dawn electric
371 field plays an essential role in ions energization.

372

373 **Acknowledgements**

374 Our work was supported by the National Natural Science Foundation of
375 China (NSFC) under grants 41474144, 41674176, and 41474124, and the
376 fund of the Lunar and Planetary Science Laboratory, Macau University of
377 Science and Technology – Partner Laboratory of Key Laboratory of
378 Lunar and Deep Space Exploration, Chinese Academy of Sciences
379 (FDCT No. 039/2013/A2). The simulation data will be made available up
380 on request by contacting Haoyu Lu.



381

382 **Reference**

383 Angelopoulos, V., Kennel, C. F., Coroniti, F. V., Pellat, R., Kivelson, M.

384 G., Walker, R. J., Russell, C. T., Baumjohann, W., Feldman, W. C., and

385 Gosling, J. T.: Statistical characteristics of bursty bulk flow events, J.

386 Geophys. Res., 99(A11), 21,257–21,280, 1994.

387 Artemyev, A. V., Liu, J., Angelopoulos, V., and Runov, A.: Acceleration

388 of ions by electric field pulses in the inner magnetosphere, J. Geophys.

389 Res. Space Physics, 120, 4628–4640, 2015.

390 Artemyev, A. V., Lutsenko, V. N., and Petrukovich, A. A.: Ion resonance

391 acceleration by dipolarization fronts: Analytic theory and spacecraft

392 observation, Ann. Geophys., 30, 317–324, 2012.

393 Artemyev, A. V., Baumjohann, W., Petrukovich, A. A., Nakamura, R.,

394 Dandouras, I., and Fazakerley, A.: Proton/electron temperature ratio in

395 the magnetotail, Ann. Geophys., 29, 2253–2257, 2011.

396 Artemyev, A. V., Zimbardo, G., A. Ukhorskiy, Y., and Fujimoto, M.:

397 Preferential acceleration of heavy ions in the reconnection outflow

398 region. Drift and surfatron ion acceleration, Astron. Astrophys., 562,

399 A58, 2014.

400 Baumjohann, W., Paschmann, G., and Cattell, C. A.: Average plasma

401 properties in the central plasma sheet, J. Geophys. Res., 94, 6597–6606,

402 1989.



- 403 Birn, J., Runov, A., and Hesse, M.: Energetic ions in dipolarization events,
 404 J. Geophys. Res. Space Physics, 120, 7698–7717, 2015.
- 405 Birn, J., Artemyev, A. V., Baker, D. N., Echim, M., Hoshino, M., and
 406 Zelenyi, L. M.: Particle acceleration in the magnetotail and aurora,
 407 Space Sci. Rev., 173, 49–102, 2012.
- 408 Birn, J., Thomsen, M. F., and Hesse M.: Electron acceleration in the
 409 dynamic magnetotail: Test particle orbits in three-dimensional MHD
 410 simulation fields, Phys. Plasmas, 11, 1825–1833, 2004.
- 411 Birn, J., Hesse, M., Nakamura, R., and Zaharia, S.: Particle acceleration
 412 in dipolarization events, J. Geophys. Res. Space Physics, 118, 1960–
 413 1971, 2013.
- 414 Birn, J., Nakamura, R., Panov, E. V., and Hesse, M.: Bursty bulk flows
 415 and dipolarization in MHD simulations of magnetotail reconnection, J.
 416 Geophys. Res., 116, A01210, 2011.
- 417 Fu, H. S., Khotyaintsev, Y. V., Vaivads, A., André, M., and Huang, S. Y.:
 418 Occurrence rate of earthward-propagating dipolarization fronts,
 419 Geophys. Res. Lett., 39, L10101, 2012a.
- 420 Fu, H. S., Khotyaintsev, Y. V., Vaivads, A., André, M., and Huang, S. Y.:
 421 Electric structure of dipolarization front at sub-proton scale, Geophys.
 422 Res. Lett., 39, L06105, 2012b.
- 423 Fu, H. S., Khotyaintsev, Y. V., André, M., and Vaivads, A.: Fermi and
 424 betatron acceleration of suprathermal electrons behind dipolarization



- 425 fronts, *Geophys. Res. Lett.*, 38, L16104, 2011.
- 426 Fu, H. S., Cao, J. B., Khotyaintsev, Y. V., Sitnov, M. I., Runov, A.,
427 Fu, S. Y., Hamrin, M., André, M., Retinò, A., Ma, Y. D., Lu, H. Y.,
428 Wei, X. H., and Huang, S. Y.: Dipolarization fronts as a consequence of
429 transient reconnection: In situ evidence, *Geophys. Res. Lett.*, 40, 6023–
430 6027, 2013.
- 431 Ge, Y. S., Raeder, J., Angelopoulos, V., Gilson, M. L., and Runov, A.:
432 Interaction of dipolarization fronts within multiple bursty bulk flows in
433 global MHD simulations of a substorm on 27 February 2009, *J.*
434 *Geophys. Res.*, 116, A00I23, 2011.
- 435 Greco, A., Artemyev, A., and Zimbardo, G.: Proton acceleration at
436 two-dimensional dipolarization fronts in the magnetotail, *J. Geophys.*
437 *Res. Space Physics*, 119, 8929–8941, 2014.
- 438 Guzdar, P. N., Hassam, A. B., Swisdak, M., and Sitnov, M. I.: A simple
439 MHD model for the formation of multiple dipolarization fronts,
440 *Geophys. Res. Lett.*, 37, L20102, 2010.
- 441 Huang, S. Y., Yuan, Z. G., Ni, B., Zhou, M., Fu, H. S., Fu, S., Deng, X. H.,
442 Pang, Y., Li, H. M., Wang, D. D., Li, H. M., Yu, X. D.: Observations of
443 large-amplitude electromagnetic waves and associated wave-particle
444 interactions at the dipolarization front in the Earth's magnetotail: A
445 case study, *J. Atmos. Sol. Terr. Phys.*, 129, 119–127, 2015.
- 446 Kiehas, S. A., Semenov, V. S., Kubyshkina, M. V., Angelopoulos, V.,



- 447 Nakamura, R., Keika, K., Ivanova, V. V., Biernat, H. K., Baumjohann,
448 W., Mende, S., Magnes, W., Auster, U., Fornaçon, K.-H., Larson, D.,
449 Carlson, C. W., Bonnell, J., McFadden, J.: First application of a
450 Petschek-type reconnection model with time-varying reconnection rate
451 to THEMIS observations, *J. Geophys. Res.*, 114, A00C20, 2009.
- 452 Li, S.-S., Angelopoulos, V., Runov, A., Zhou, X.-Z., McFadden, J.,
453 Larson, D., Bonnell, J., and Auster, U.: On the force balance around
454 dipolarization fronts within bursty bulk flows, *J. Geophys. Res.*, 116,
455 A00I35, 2011.
- 456 Lu, H. Y., Cao, J. B., Zhou, M., Fu, H. S., Nakamura, R., Zhang, T. L.,
457 Khotyaintsev, Y. V., Ma, Y. D., and Tao, D.: Electric structure of
458 dipolarization fronts associated with interchange instability in the
459 magnetotail, *J. Geophys. Res. Space Physics*, 118, 2013.
- 460 Lu, H. Y., Cao, J. B., Ge, Y. S., Zhang, T. L., Nakamura, R., and Dunlop,
461 M. W.: Hall and finite Larmor radius effects on the dipolarization
462 fronts associated with interchange instability, *Geophys. Res. Lett.*, 42,
463 2015.
- 464 Lu, H.Y., Li, Y., Cao, J., Ge, Y., Zhang, T., and Yu, Y.: Numerical
465 simulation on the multiple dipolarization fronts in the magnetotail,
466 *Phys. Plasmas* 24, 102903 2017.
- 467 Nakamura, R., Baumjohann, W., Klecker, B., Bogdanova, Y., Balogh, A.,
468 Remé, H., Bosqued, J., Dandouras, I., Sauvaud, J., Glassmeier, K.,



- 469 Kistler, L., Mouikis, C., Zhang, T., Eichelberger, H. and Runov, A.:
470 Motion of the dipolarization front during a flow burst event observed
471 by Cluster, Geophys. Res. Lett., 29(20), 1942, 2002.
- 472 Nakamura, R., Retinò, A., Baumjohann, W., Volwerk, M., Erkaev, N.,
473 Klecker, B., Lucek, E. A., Dandouras, I., André, M., Khotyaintsev, Y.:
474 Evolution of dipolarization in the near-Earth current sheet induced by
475 Earthward rapid flux transport, Ann. Geophys., 27, 1743–1754, 2009.
- 476
- 477 Nakamura, R., Baumjohann, W., Panov, E., Volwerk, M., Birn, J.,
478 Artemyev, A., Petrukovich, A. A., Amm, O., Juusola, L., Kubyshkina,
479 M. V., Apatenkov, S., Kronberg, E. A., Daly, P. W., Fillingim, M.,
480 Weygand, J. M., Fazakerley, A., Khotyaintsev, Y.: Flow bouncing and
481 electron injection observed by Cluster, J. Geophys. Res. Space Physics,
482 118, 2055–2072, 2013.
- 483 Ohtani, S. I., Shay, M. A., and Mukai, T.: Temporal structure of the fast
484 convective flow in the plasma sheet: Comparison between observations
485 and two-fluid simulations, J. Geophys. Res., 109, A03210, 2004.
- 486 Pritchett, P. L., and Coroniti, F. V.: Structure and consequences of the
487 kinetic ballooning/interchange instability in the magnetotail, J.
488 Geophys. Res. Space Physics, 118, 146-159, 2013.
- 489 Runov, A., Angelopoulos, V., Sitnov, M. I., Sergeev, V. A., Bonnell J.,
490 McFadden, J. P., Larson, D., Glassmeier, K.-H., and Auster, U.:



- 491 THEMIS observations of an earthward-propagating dipolarization front,
492 Geophys. Res. Lett, 36, L14106, 2009.
- 493 Runov, A., Angelopoulos, V., Zhou, X.-Z., Zhang, X.-J., Li, S., Plaschke,
494 F., and Bonnell, J.: A THEMIS multicasestudy of dipolarization fronts
495 in the magnetotail plasma sheet, J. Geophys. Res., 116, A05216, 2011.
- 496 Schmid, D., et al. (), A comparative study of dipolarization fronts at MMS
497 and Cluster, Geophys. Res. Lett., 43, 6012–6019, 20160.
- 498 Schmid, D., Volwerk, M., Nakamura, R., Baumjohann, W., and Heyn, M.:
499 A statistical and event study of magnetotail dipolarization fronts, Ann.
500 Geophys., 29, 1537–1547, 2011.
- 501 Sitnov, M. I., Swisdak, M., and Divin, A. V.: Dipolarization fronts as a
502 signature of transient reconnection in the magnetotail, J. Geophys. Res.,
503 114, A04202, 2009.
- 504 Ukhorskiy, A. Y., Sitnov, M. I., Merkin, V. G., and Artemyev, A. V.: Rapid
505 acceleration of protons upstream of earthward propagating
506 dipolarization fronts, J. Geophys. Res. Space Physics, 118, 4952–4962,
507 2013.
- 508 Ukhorskiy, A. Y., Sitnov, M. I., Merkin, V. G., Gkioulidou, M., and
509 Mitchell, D. G.: Ion acceleration at dipolarization fronts in the inner
510 magnetosphere, J. Geophys. Res. Space Physics, 122, 3040–3054,
511 2017.
- 512 Zhou, M., Huang, S.-Y., Deng, X.-H., and Pang, Y.: Observation of a



513 sharp negative dipolarization front in the reconnection outflow region,
514 Chin. Phys. Lett., 28(10), 109402, 2011.
515 Zhou, X.-Z., Angelopoulos, V., Liu, J., Runov, A., and Li, S.-S.: On the
516 origin of pressure and magnetic perturbations ahead of dipolarization
517 fronts, J. Geophys. Res. Space Physics, 119,211–220, 2014.
518 Zhou, X. - Z., Angelopoulos, V., Sergeev, V. A., and Runov, A.:
519 Accelerated ions ahead of earthward propagating dipolarization fronts, J.
520 Geophys. Res., 115, A00I03, 2010.
521 Zhou, X.-Z., Angelopoulos, V., Sergeev, V. A., and Runov, A.: On the
522 nature of precursor flows upstream of advancing dipolarization fronts,
523 J. Geophys. Res., 116, A03222, 2011.
524